Available online at www.sciencedirect.com
ScienceDirect
Journal of Sound and Vibration 324 (2009) 1067–1085
JOURNAL OF SOUND AND VIBRATION
www.elsevier.com/locate/jsvi

Triply coupled bending–torsion vibration of Timoshenko and Euler–Bernoulli shaft beams with arbitrarily oriented open crack

Sachin S. Naik, Surjya K. Maiti*

Mechanical Engineering Department, Indian Institute of Technology Bombay, Mumbai 400 076, India

Received 3 August 2008; received in revised form 9 December 2008; accepted 15 February 2009
Handling Editor: L.G. Tham
Available online 28 March 2009

Abstract

The paper presents the full formulation for a crack model for analyzing the triply coupled free vibration of both Timoshenko (short) and Euler–Bernoulli (long) shaft beams based on compliance approach in the presence of a planar open edge crack in an arbitrary angular orientation with a reference direction. The compliance coefficients to account for the local flexibility due to the crack for both the beams have been obtained through the concept of strain energy release rate and crack tip stress field given in terms of the stress intensity factors. The type of disturbance in stress–strain field that a continuous cracked beam theory can accommodate is not within the scope of the model. The compliance matrices for the Timoshenko (short) and Euler–Bernoulli (long) beams, respectively, are of size 6×6 and 3×3, and they consist of only 9 and 4 nonzero coefficients. The variation of the coefficients with crack orientation is presented. Equations governing the free transverse and torsion vibrations are derived and solved in both the cases. The formulation has been checked by comparing the theoretical frequencies with the finite element results for a few crack orientations, locations and depths. The agreement is good. It is shown further that, when such cases are analysed for studying the transverse vibration only in one plane by invoking a single rotational spring at the crack location, the approach leads to an erroneous variation of the frequencies with the crack orientations. The data presented here will be useful to solve both forward and inverse problems.

1. Introduction

During the last three decades detection of crack in machine and structrural components has received a considerable attention. Excellent reviews are presented by Wauer [1], Gasch [2], Dimarogonas [3] and Papadopoulos [4]. These indicate clearly that the modelling of a crack is the most significant issue in this area. Dimarogonas and Massouros [5] combined the spring-hinge, or the rotational spring, model with fracture mechanics based results to evolve an attractive method for crack identification. This idea was further extended to cover cases with arbitrary loading by Papadopoulos and Dimarogonas [6]. If the crack opens and closes during the rotation the system becomes nonlinear. This makes the component response complicated. In the case of rotors, two families of harmonics are observed on top of the second harmonic of rotation and the

*Corresponding author. Tel.: +91 22 2576 7526; fax: +91 22 2572 6875.
E-mail address: skmaiti@me.iitb.ac.in (S.K. Maiti).

0022-460X/$ - see front matter © 2009 Elsevier Ltd. All rights reserved.
doi:10.1016/j.jsv.2009.02.015

sub-harmonic of the critical speed. The first concerns higher harmonics of the rotating speed [3] due to the nonlinearity of the closing crack. The second includes the longitudinal and torsion harmonics in the start-up lateral vibration spectrum due to the coupling.

Darpe et al. [7,8] have investigated into the response of a Jeffcott rotor to axial excitation of different frequencies. They have observed based on both theoretical and experimental studies clear differences in the frequency spectra of the rotor with and without crack. These differences can be utilised to confirm the presence of a crack. Darpe et al. [9] too have investigated into the coupled longitudinal, lateral and torsion vibration for a rotating shaft using a response dependent nonlinear breathing crack. They reported presence of sums or/and differences of frequencies in the vibration spectra arising out of the nonlinearity.

Flaws/cracks developing in a component during service may seriously influence its dynamic behaviour. These may cause changes in its mass distribution and damping properties. The crack may also modify the stress–strain field over a larger distance than covered by a solution based on the stress intensity factor. In such cases continuous cracked beam approach based on the Hu–Washizu or Hu–Washizu–Barr variational statement presented by Christides and Barr [10,11], Shen and Pierre [12], Chandros [13,14], Chandros and Labeas [15], etc., may be more appropriate for obtaining the natural frequencies with better accuracy.

A crack can be modeled as an 'open' or 'breathing' crack. In the case of open crack model the local flexibility can be represented by a flexibility matrix [6] of dimension (6×6) under the most general loading. An important review concerning determination of local flexibility coefficients/matrix in the presence of a single crack based on the concept of strain energy release rate has been recently presented by Papadopoulos [4]. For some cases simplification is possible and the local flexibility can be conveniently represented by a single rotational spring [4,16] or a reduction in cross-sectional dimensions [17]. The representation through the local flexibility or the rotational spring is very convenient because of its ability to facilitate solution of an inverse problem, where the crack details are to be determined knowing the component vibration response. On the other hand, in the solution to a forward problem, system eigenfrequencies, mode shapes, etc., are predicted with the knowledge of crack details, e.g., crack location, depth and orientation angle.

Lele and Maiti [18] have solved both the forward and inverse problems associated with a Timoshenko beam of rectangular cross-section with an open edge crack. The beam vibrates only in one of the planes of symmetry. They have represented the crack by a rotational spring. Dharmaraju et al. [19] have developed a general algorithm for estimation of crack depth using experimentally measured forced vibration response. They have used an Euler–Bernoulli beam element to model the beam of circular cross section through finite element method (FEM). The crack is considered in the vertical orientation and has been modeled by a local compliance matrix. The coupled response in the vertical and horizontal directions is used to identify the crack parameters.

Dado and Abuzeid [20] have presented the vibration behaviour of an Euler–Bernoulli beam of rectangular cross section with end mass and rotary inertia. They have studied the coupled longitudinal and transverse vibrations using the compliance approach. Ostachowicz and Krawczuk [21] have developed a special finite element (FE) to represent a segment of shaft beam with an open edge crack in the vertical orientation. They have formulated for coupled bending and torsion vibrations for a Timoshenko beam and employed the compliance approach to determine flexibility matrix of the special element. Darpe et al. [9] have extended the approach of Ostachowicz and Krawczuk [21] to account for additional longitudinal coupling for a breathing crack in the same orientation. The coupling of transverse vibrations for long beam of solid circular section is addressed by Chasalevris and Papadopoulos [22]. Problem involving hollow circular and rectangular section has been examined by Zheng and Fan [23], and Gounaris et al. [24]. A method for identification of location and depth of the edge crack using the measured coupled vibration response has been presented by Gounaris and Papadopoulos [25]. They have given a cracked circular element, with 12 degrees of freedom per element, for analysing a Timoshenko shaft beam. The model is capable of accommodating gyroscopic effect as well. Chondros et al. [26] have employed a continuous cracked beam theory for prediction of changes in the transverse natural frequencies for a simply supported beam with a breathing crack. The crack is modeled as a continuous flexibility through a displacement field in the vicinity of the crack. Both bilinear and linear models are considered to study the problem. They have reported that changes in natural frequencies for a fatigue-breathing crack are smaller than those due to an open crack. That is, the open crack model over-predicts the changes in the lowest natural frequency.

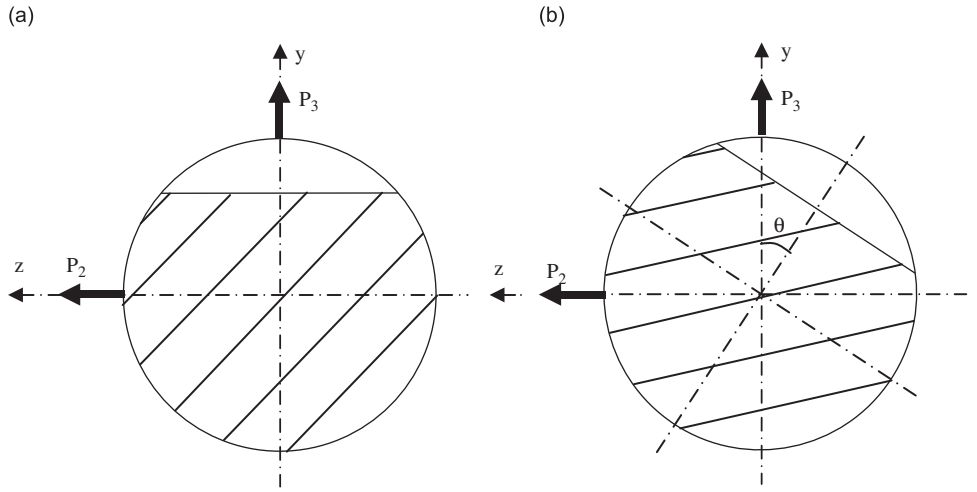

Fig. 1. Crack in two different orientations. (a) $\theta = 0^\circ$ and (b) arbitrary θ.

Zheng and Kessissoglou [27] have established a scheme to obtain the natural frequencies and mode shapes of a beam through the FEM. They have introduced the artefact of an 'overall additional flexibility matrix' to the intact beam flexibility matrix to account for the crack. They have claimed that the method gives results more accurate than those obtained by the concept of local flexibility matrix.

Most studies consider the case of a vertical crack (Fig. 1a) giving rise to coupled transverse and torsion vibrations. A crack due to a manufacturing defect, and/or service loading, and/or environment, can occur in an arbitrary orientation (Fig. 1b) in the case of non-rotating component. Alternatively, the response collected from a rotating system may correspond to an arbitrary angular crack orientation with respect to, say, the vertical direction. There is, therefore, a need to study both the forward and inverse problem solutions associated with such a situation.

In the present paper a solution to the triply coupled forward vibration problem is attempted based on the localised compliance approach to model a crack. It is relevant to note here that the inverse problem of this type has been studied by Naniwadekar et al. [28] considering a single rotational spring based representation of the crack in pipes. The spring stiffness was obtained experimentally. They have been able to predict the crack location and the size. Chasalevris and Papadopoulos [22] have solved both the forward and inverse problems for a shaft with two arbitrarily oriented cracks in an Euler–Bernoulli beam using the compliance approach. The situation gives rise to coupled transverse vibration in the two orthogonal directions. The prediction of crack is based on wavelet transformation of the response. Saridakis et al. [29] have extended the same study further to compute natural frequencies in both the vertical and horizontal directions. They solved the related inverse problem through a fuzzy logic and genetic algorithm based optimization method.

2. Local compliance coefficients

When a crack is oriented at $\theta = 0^\circ$ (Fig. 1a), load P_2 in z direction does not lead to any crack face relative displacement in direction y and vice versa [6]. On the other hand, for an angular orientation of the crack (Fig. 1b) P_2 applied in z direction gives rise to the displacement in y direction and vice versa. In this case not only the compliance coefficients c_{22} or c_{33} but also c_{23} is greater than zero.

For a shaft beam, noting that P_2 and P_3 cause mode III and mode II (Fig. 1a) crack face displacements, respectively, the same loads in the presence of an angularly oriented crack (Fig. 1b) give rise to both the modes of displacements simultaneously. Hence each of the three compliance coefficients will have contribution from both the modes (II and III).

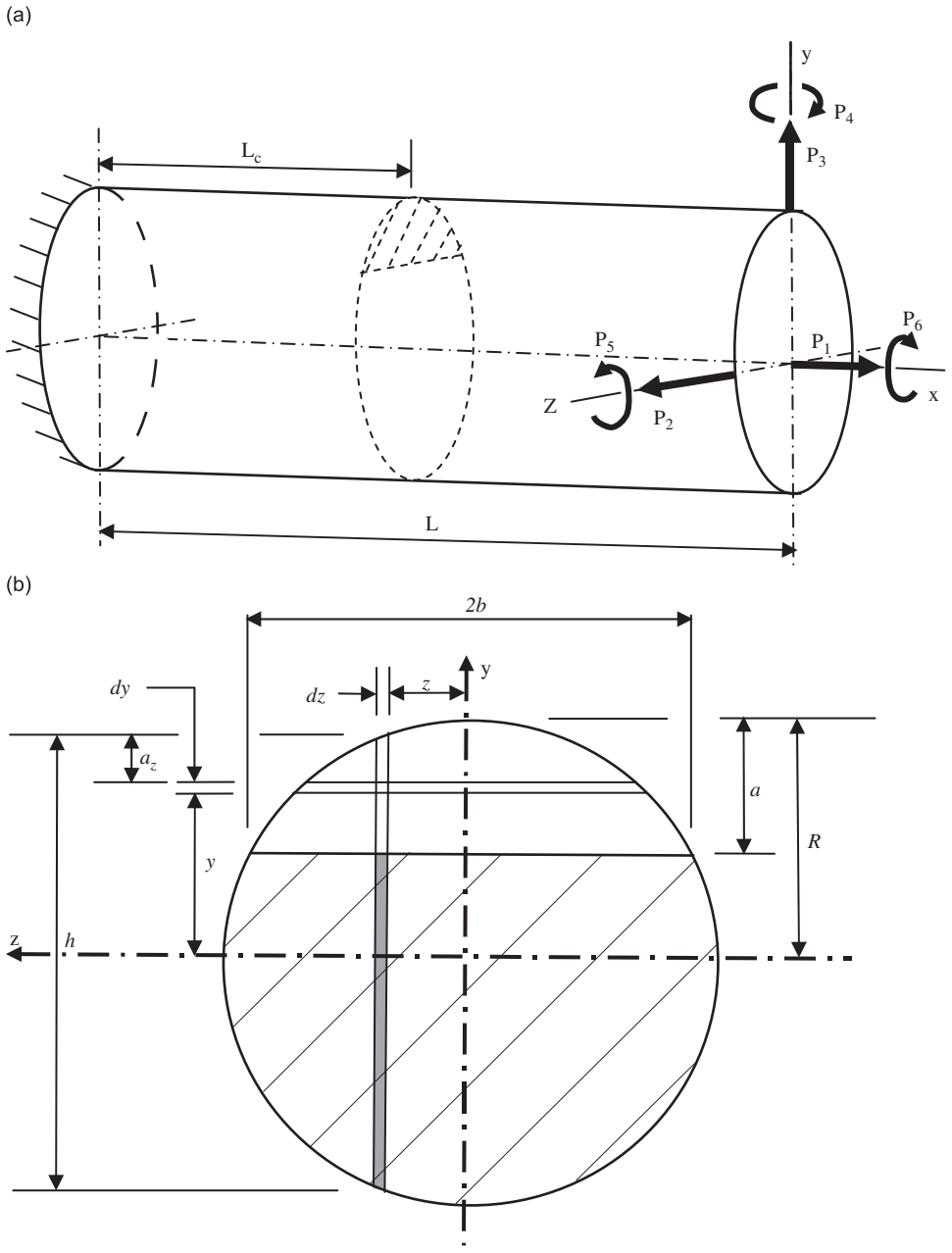

Fig. 2. (a) Crack in 0° orientation and (b) crack section geometry.

In the most general case of loading (Fig. 2a) and a crack in 0° orientation, the compliance coefficients are given in Ref. [6].

With an angular crack orientation θ (Fig. 3a) the components of loads in the y_1–z_1 system, represented by an additional subscript θ, are given by

$$\left.\begin{aligned} P_{3\theta} &= P_3 \cos\theta - P_2 \sin\theta \\ P_{2\theta} &= P_3 \sin\theta + P_2 \cos\theta \\ P_{4\theta} &= -P_4 \cos\theta - P_5 \sin\theta \\ P_{5\theta} &= -P_4 \sin\theta + P_5 \cos\theta \end{aligned}\right\} \tag{1}$$

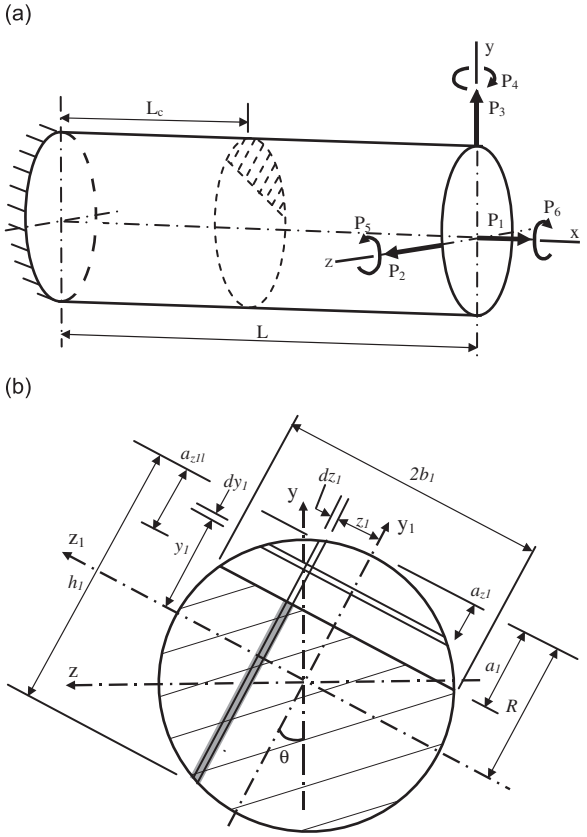

Fig. 3. (a) Shaft with arbitrarily oriented crack and (b) crack section geometry.

Adopting the approach similar to Papadopoulos and Dimarogonas [6], additional crack face relative displacement u_i, $i = 2, 3, \ldots, 6$, along the direction of P_i due to the presence of a crack of depth a_1 is obtained through integration.

$$u_i = \frac{\partial}{\partial P_i} \int_0^A J \, \mathrm{d}A \tag{2}$$

where J is the local strain energy release rate, $\mathrm{d}A = \mathrm{d}y_1 \, \mathrm{d}z_1$ (Fig. 3b) and A is area of crack. Note that u_i is displacement in the ith direction in y–z system. Under a combined loading J is given by

$$J = \frac{1}{E'} \left[\left(\sum_{i=1}^{6} K_{\mathrm{I}i} \right)^2 + \left(\sum_{i=1}^{6} K_{\mathrm{II}i} \right)^2 + (1+\nu) \left(\sum_{i=1}^{6} K_{\mathrm{III}i} \right)^2 \right] \tag{3}$$

where $E' = E$ for plane stress, $E' = E/(1-\nu^2)$ for plane strain, E is modulus of elasticity, ν is the Poisson's ratio and $K_{\mathrm{I}i}$, $K_{\mathrm{II}i}$, $K_{\mathrm{III}i}$ are the SIFs for modes I, II and III corresponding to loads $P_{i\theta}$. The energy calculation is facilitated by taking $y_1 - z_1$ as reference. For a shaft beam, computation of J is facilitated [6] by dividing the whole span $2b_1$ into a number of strips of thickness $\mathrm{d}z_1$ and considering each of them to be under plane strain. Noting that the local flexibility $c'_{ij\theta}$ due to the crack per unit width is given [6] by

$$c'_{ij\theta} = \frac{\partial u_i}{\partial P_j} = \frac{\partial^2}{\partial P_i \, \partial P_j} \int_{a_{z1l}} J \, \mathrm{d}a_{z1} \tag{4}$$

Total compliance is obtained as follows:

$$c_{ij\theta} = \frac{\partial^2}{\partial P_i \partial P_j}\int_0^A J\,\mathrm{d}A = \frac{\partial^2}{\partial P_i \partial P_j}\int_{-b_1}^{b_1}\int_{a_{z1l}} J(a_{z1})\,\mathrm{d}y_1\,\mathrm{d}z_1 \tag{5}$$

where $a_{z1} = \frac{h}{2} - y_1$.

To differentiate c_{ij}'s corresponding to $\theta = 0^\circ$ and $\theta \neq 0^\circ$, θ is added as a subscript in the latter case. Though the additional displacements are calculated in y–z coordinates, the strain energy and strain energy release rate J computation is facilitated by taking y_1–z_1 coordinates as the basis. The nonzero coefficients in dimensionless form are given below:

$$\bar{c}_{11\theta} = \frac{\pi E R c_{11\theta}}{1-\nu^2} = 4\int_0^{\bar{b}_1}\int_{a_{z1l}} \bar{y}_1 F_1^2\left(\frac{\bar{a}_{z1}}{\bar{h}_1}\right)\mathrm{d}\bar{y}_1\,\mathrm{d}\bar{z}_1 \tag{6}$$

$$\bar{c}_{14\theta} = \frac{\pi E R^2 c_{14\theta}}{1-\nu^2} = 8\cos\theta\int_0^{\bar{b}_1}\int_{a_{z1l}} \bar{z}_1\bar{y}_1 F_1^2\left(\frac{\bar{a}_{z1}}{\bar{h}_1}\right)\mathrm{d}\bar{y}_1\,\mathrm{d}\bar{z}_1 \tag{7}$$

$$\bar{c}_{15\theta} = \frac{\pi E R^2 c_{15\theta}}{1-\nu^2} = 16\cos\theta\int_0^{\bar{b}_1}\int_{a_{z1l}} \bar{y}_1\sqrt{1-\bar{z}^2}F_1\left(\frac{\bar{a}_{z1}}{\bar{h}_1}\right)F_2\left(\frac{\bar{a}_{z1}}{\bar{h}_1}\right)\mathrm{d}\bar{y}_1\,\mathrm{d}\bar{z}_1 \tag{8}$$

where F_1 and F_2 are SIF correction factors given in Ref. [6]. As indicated earlier, for calculations of shear mode coefficients $c_{22\theta}$, $c_{33\theta}$ and $c_{23\theta}$, contributions to strain energy release rate from both crack face displacement modes II and III must be considered. That is,

$$\bar{c}_{22\theta} = \frac{\pi E R c_{22\theta}}{1-\nu^2} = 4\int_0^{\bar{b}_1}\int_{a_{z1l}} \bar{y}_1 k'^2\left(F_{II}^2\left(\frac{\bar{a}_{z1}}{\bar{h}_1}\right)\sin^2\theta + mF_{III}^2\left(\frac{\bar{a}_{z1}}{\bar{h}_1}\right)\cos^2\theta\right)d\bar{y}_1\,d\bar{z}_1 \tag{9}$$

$$\bar{c}_{33\theta} = \frac{\pi E R c_{33\theta}}{1-\nu^2} = 4\int_0^{\bar{b}_1}\int_{a_{z1l}} \bar{y}_1 k'^2\left(F_{II}^2\left(\frac{\bar{a}_{z1}}{\bar{h}_1}\right)\cos^2\theta + mF_{III}^2\left(\frac{\bar{a}_{z1}}{\bar{h}_1}\right)\sin^2\theta\right)d\bar{y}_1\,d\bar{z}_1 \tag{10}$$

$$\bar{c}_{23\theta} = \frac{\pi E R c_{23\theta}}{1-\nu^2} = 4\int_0^{\bar{b}_1}\int_{a_{z1l}} \bar{y}_1 K'^2\left(\left(mF_{III}^2\left(\frac{\bar{a}_{z1}}{\bar{h}_1}\right) - F_{II}^2\left(\frac{\bar{a}_{z1}}{\bar{h}_1}\right)\right)\sin\theta\cos\theta\right)d\bar{y}_1\,d\bar{z}_1 \tag{11}$$

where F_{II} and F_{III} are correction factors indicated in Ref. [6]. For calculating F_{III} it is more appropriate to use the average shear stress over the crack depth rather than the maximum, as indicated by Ref. [6]. Further, for the bending compliance coefficients $c_{44\theta}$ and $c_{55\theta}$ contributions to the strain energy release rate from both the loads P_4 and P_5 (Fig. 3a) must be considered:

$$\bar{c}_{44\theta} = \frac{\pi E R^3 c_{44\theta}}{1-\nu^2} = 64\int_0^{\bar{b}_1}\int_{a_{z1l}} (A_1\cos^2\theta + B_1\sin^2\theta - C_1\sin\theta\cos\theta)\,\mathrm{d}\bar{y}_1\,\mathrm{d}\bar{z}_1 \tag{12}$$

$$\bar{c}_{55\theta} = \frac{\pi E R^3 c_{55\theta}}{1-\nu^2} = 64\int_0^{\bar{b}_1}\int_{a_{z1l}} (A_1\sin^2\theta + B_1\cos^2\theta + C_1\sin\theta\cos\theta)\,\mathrm{d}\bar{y}_1\,\mathrm{d}\bar{z}_1 \tag{13}$$

$$\bar{c}_{45\theta} = \frac{\pi E R^3 c_{45\theta}}{1-\nu^2} = 64\int_0^{\bar{b}_1}\int_{a_{z1l}} (\sin\theta\cos\theta(A_1 - B_1) + C_1(\cos^2\theta - \sin^2\theta))\,\mathrm{d}\bar{y}_1\,\mathrm{d}\bar{z}_1 \tag{14}$$

where

$$A_1 = \bar{z}_1^2\bar{y}_1 F_1^2\left(\frac{\bar{a}_{z_1}}{\bar{h}_1}\right);\quad B_1 = (1-\bar{z}_1^2)\bar{y}_1 F_2^2\left(\frac{\bar{a}_{z1}}{\bar{h}_1}\right);\quad C_1 = \bar{z}_1\bar{y}_1\sqrt{1-\bar{z}_1^2}F_1\left(\frac{\bar{a}_{z1}}{\bar{h}_1}\right)F_2\left(\frac{\bar{a}_{z1}}{\bar{h}_1}\right)$$

In case of a fatigue-breathing crack, the integration associated with Eqs. (12)–(14) are to be done from 0 to $\bar{b}_1$ only [30].

The other nonzero compliance coefficients are computed through the following relations:

$$\bar{c}_{66\theta} = \frac{\pi E R^3 c_{66\theta}}{1-\nu^2} = 16 \int_0^{\bar{h}_1} \int_{\bar{a}_{z1l}} \bar{y}_1 \left(\bar{z}_1^2 F_{\mathrm{II}}^2 \left(\frac{\bar{a}_{z1}}{\bar{h}_1} \right) + m(1-\bar{z}_1^2) F_{\mathrm{III}t}^2 \left(\frac{\bar{a}_{z1}}{\bar{h}_1} \right) \right) \mathrm{d}\bar{y}_1 \, \mathrm{d}\bar{z}_1 \tag{15}$$

$$\bar{c}_{26\theta} = \frac{\pi E R^2 c_{26\theta}}{1-\nu^2} = 8 \int_0^{\bar{h}_1} \int_{\bar{a}_{z1l}} \bar{y}_1 k' \left(-z_1 F_{\mathrm{II}}^2 \left(\frac{\bar{a}_{z1}}{\bar{h}_1} \right) \sin\theta - m\sqrt{(1-\bar{z}_1^2)} F_{\mathrm{III}} \left(\frac{\bar{a}_{z1}}{\bar{h}_1} \right) F_{\mathrm{III}t} \left(\frac{\bar{a}_{z1}}{\bar{h}_1} \right) \cos\theta \right) \mathrm{d}\bar{y}_1 \, \mathrm{d}\bar{z}_1 \tag{16}$$

$$\bar{c}_{36\theta} = \frac{\pi E R^2 c_{36\theta}}{1-\nu^2} = 8 \int_0^{\bar{h}_1} \int_{\bar{a}_{z1l}} \bar{y}_1 \left(\bar{z}_1 F_{\mathrm{II}}^2 \left(\frac{\bar{a}_{z1}}{\bar{h}_1} \right) \cos\theta - m\sqrt{(1-\bar{z}_1^2)} F_{\mathrm{III}} \left(\frac{\bar{a}_{z1}}{\bar{h}_1} \right) F_{\mathrm{III}t} \left(\frac{\bar{a}_{z1}}{\bar{h}_1} \right) \sin\theta \right) \mathrm{d}\bar{y}_1 \, \mathrm{d}\bar{z}_1 \tag{17}$$

where $\bar{z}_1 = z_1/R$, $\bar{y}_1 = y_1/R$, $\bar{a}_{z1} = a_{z1}/R$, $\bar{h}_1 = h_1/R$, $m = (1+\nu)$. $F_{\mathrm{III}t}$ indicates the correction factor with the consideration of average shear stress over the crack depth. It may be noted that the angular orientation of the crack does not affect the longitudinal and torsion compliances. Therefore, $\bar{c}_{11\theta} = \bar{c}_{11}$ and $\bar{c}_{66\theta} = \bar{c}_{66}$.

Finally, the full (6×6) symmetric dimensionless compliance matrix for the shaft beam is as follows:

$$\bar{c}_{ij\theta} = \begin{bmatrix} \bar{c}_{11\theta} & 0 & 0 & \bar{c}_{14\theta} & \bar{c}_{15\theta} & 0 \\ 0 & \bar{c}_{22\theta} & \bar{c}_{23\theta} & 0 & 0 & \bar{c}_{26\theta} \\ 0 & \bar{c}_{32\theta} & \bar{c}_{33\theta} & 0 & 0 & \bar{c}_{36\theta} \\ \bar{c}_{41\theta} & 0 & 0 & \bar{c}_{44\theta} & \bar{c}_{45\theta} & 0 \\ \bar{c}_{51\theta} & 0 & 0 & \bar{c}_{54\theta} & \bar{c}_{55\theta} & 0 \\ 0 & \bar{c}_{62\theta} & \bar{c}_{63\theta} & 0 & 0 & \bar{c}_{66\theta} \end{bmatrix} \tag{18}$$

The dimensionless compliance matrix for a Timoshenko beam subjected to all loads but P_1 is given by

$$\bar{c}_{ij\theta} = \begin{bmatrix} \bar{c}_{22\theta} & \bar{c}_{23\theta} & 0 & 0 & \bar{c}_{26\theta} \\ \bar{c}_{32\theta} & \bar{c}_{33\theta} & 0 & 0 & \bar{c}_{36\theta} \\ 0 & 0 & \bar{c}_{44\theta} & \bar{c}_{45\theta} & 0 \\ 0 & 0 & \bar{c}_{54\theta} & \bar{c}_{55\theta} & 0 \\ \bar{c}_{62\theta} & \bar{c}_{63\theta} & 0 & 0 & \bar{c}_{66\theta} \end{bmatrix} \tag{19}$$

The dimensionless compliance matrix for an Euler–Bernoulli beam is obtained by neglecting the shear related terms. That is,

$$\bar{c}_{ij\theta} = \begin{bmatrix} \bar{c}_{44\theta} & \bar{c}_{45\theta} & 0 \\ \bar{c}_{54\theta} & \bar{c}_{55\theta} & 0 \\ 0 & 0 & \bar{c}_{66\theta} \end{bmatrix} \tag{20}$$

The local stiffness coefficients can be obtained by inverting the compliance matrix.

The variations of the compliance matrix coefficients with relative crack depth (a/R) are shown in Fig. 4. Also the variations of dimensionless compliance coefficients with the crack orientation angle are shown in Fig. 5. Clearly the pairs $c_{22\theta}$ and $c_{33\theta}$, and $c_{44\theta}$ and $c_{55\theta}$, show the reciprocal behaviour with respect to crack orientation, as expected.

3. Calculation of one dimensional bending stiffness

When a beam with a crack vibrates, its motion in a single plane, say y–x plane (Fig. 6), where x is directed out of the, plane of paper, can be easily modelled by invoking a single rotational spring at the crack location. The spring stiffness can be calculated as follows. Considering only bending load P_5 (Fig. 6) acting, its componenets along z_1 and y_1 are $P_{5z1} = P_5 \cos\theta$ and $P_{5y1} = -P_5 \sin\theta$.

If the local slope discontinuities due to these moments are ϕ_{z1} and ϕ_{y1}, respectively, in y_1–z_1 system, their components along z direction are: $\phi_1 = \phi_{z1} \cos\theta$, and $\phi_2 = \phi_{y1} \sin\theta$. Writing ϕ_{z1} and ϕ_{y1} in terms

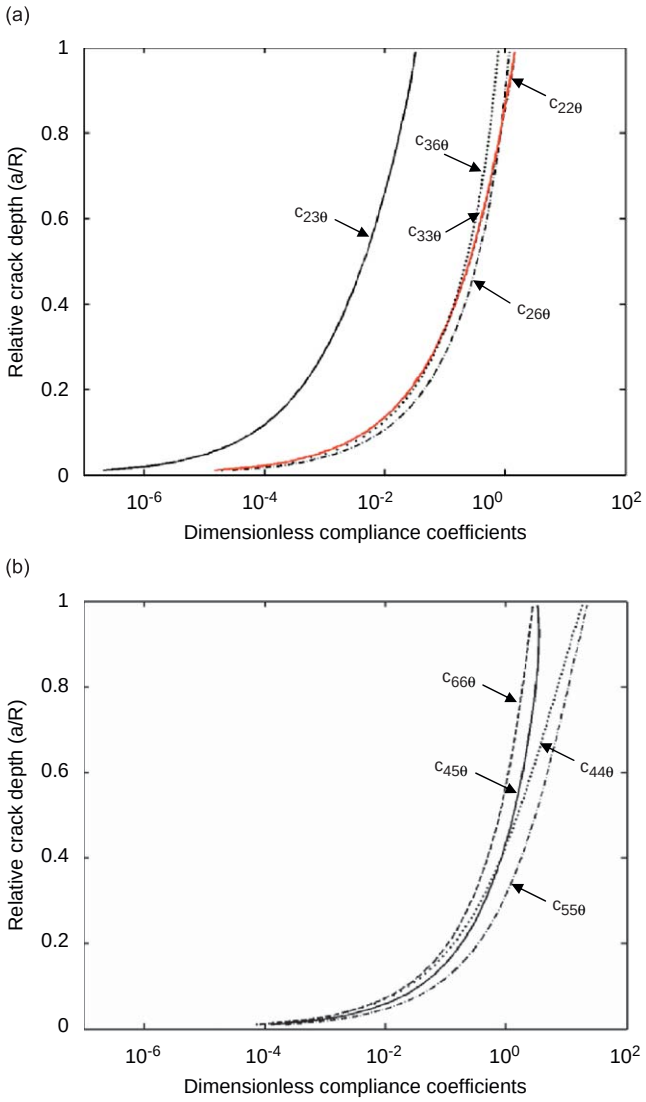

Fig. 4. Variations of dimensionless compliance coefficients with relative crack depth (a/R) for $\theta = 15^{\circ}$. (a) Variations of $c_{22\theta}$, $c_{33\theta}$, $c_{23\theta}$, $c_{26\theta}$ and $c_{36\theta}$. (b) Variations of $c_{44\theta}$, $c_{55\theta}$, $c_{45\theta}$ and $c_{66\theta}$.

of P_{5z1} and P_{5y1} and representing the corresponding rotational spring stiffnessess as K_0 and K_{90}

$$\phi_{z1} = \frac{P_{5z1}}{K_0} = \frac{P_{5z1}}{K_0}\cos\theta, \quad \phi_1 = \frac{P_5}{K_0}\cos^2\theta \tag{21}$$

$$\phi_{y1} = \frac{P_{5y1}}{K_{90}} = \frac{P_{5y1}}{K_{90}}\sin\theta, \quad \phi_2 = \frac{P_5}{K_{90}}\sin^2\theta \tag{22}$$

The total local slope discontinuity ϕ in the plane $y-x$

$$\phi = \phi_1 + \phi_2 = P_5\left(\frac{\cos^2\theta}{K_0} + \frac{\sin^2\theta}{K_{90}}\right) \tag{23}$$

This gives

$$\frac{1}{K_\theta} = \frac{\phi}{P_5} = \left(\frac{\cos^2\theta}{K_0} + \frac{\sin^2\theta}{K_{90}}\right) \tag{24}$$

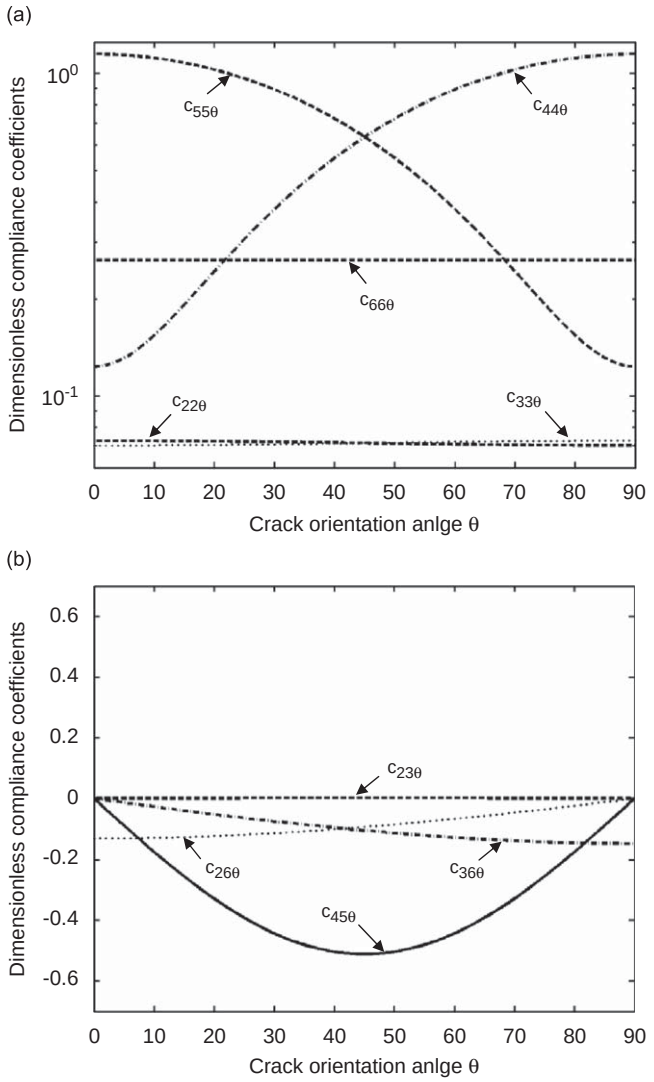

Fig. 5. Variations of dimensionless compliance coefficients with crack orientation angle θ for $(a/R) = 0.3$. (a) Variations of $c_{22\theta}$, $c_{33\theta}$, $c_{44\theta}$, $c_{55\theta}$ and $c_{66\theta}$. (b) Variations of $c_{45\theta}$, $c_{26\theta}$, $c_{36\theta}$ and $c_{23\theta}$.

Alternatively,

$$\frac{K_\theta}{K_0} = \frac{K_{90}}{K_{90}\cos^2\theta + K_0 \sin^2\theta} \tag{25}$$

In dimensionless form

$$\frac{\bar{K}_\theta}{\bar{K}_0} = \frac{\bar{K}_{90}}{\bar{K}_{90}\cos^2\theta + \bar{K}_0 \sin^2\theta} \tag{26}$$

where $\bar{K}_\theta = K_\theta L/EI$ and $\bar{K}_0 = K_0 L/EI$.

This relationship is alternatively obtainable from the rigorous relation (12) as follows. When $P_4 = 0$, Eq. (12) can be written as:

$$\begin{aligned}\bar{c}_{44\theta} = {} & \cos^2\theta \int_0^{\bar{b}_1}\int_{a_{z1l}} 64\bar{z}_1^2\bar{y}_1 F_1^2\left(\frac{\bar{a}_{z1}}{\bar{h}_1}\right)\mathrm{d}\bar{y}_1\,\mathrm{d}\bar{z}_1 + \sin^2\theta \int_0^{\bar{b}_1}\int_{a_{z1l}} 64(1-\bar{z}_1^2)\bar{y}_1 F_2^2\left(\frac{\bar{a}_{z1}}{\bar{h}_1}\right)\mathrm{d}\bar{y}_1\,\mathrm{d}\bar{z}_1 \\ & - \sin\theta\cos\theta \int_0^{\bar{b}_1}\int_{a_{z1l}} 64\bar{z}_1\bar{y}_1\sqrt{1-\bar{z}_1^2}F_1\left(\frac{\bar{a}_{z1}}{\bar{h}_1}\right)F_2\left(\frac{\bar{a}_{z1}}{\bar{h}_1}\right)\mathrm{d}\bar{y}_1\,\mathrm{d}\bar{z}\end{aligned} \tag{27}$$

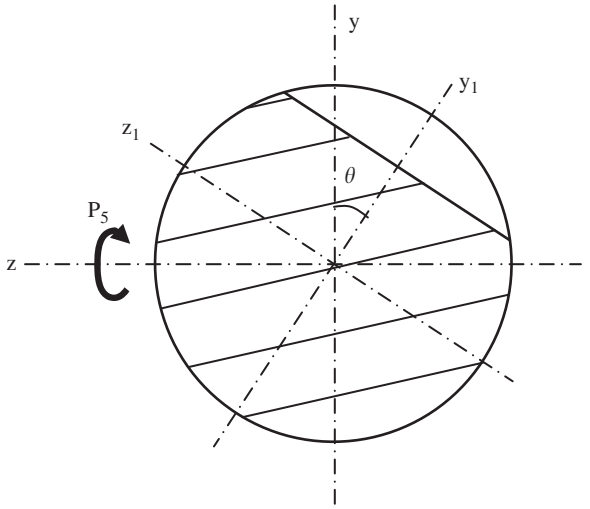

Fig. 6. Arbitrarily oriented crack subjected to moment P_5.

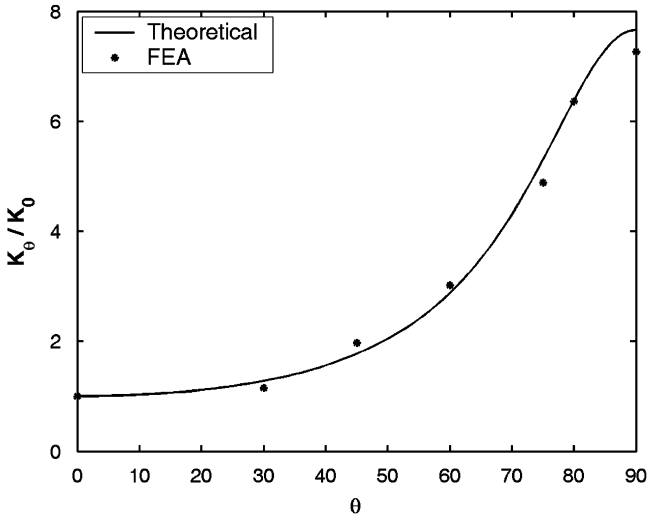

Fig. 7. Comparison of theoretical and finite element based variations of stiffness ratio (K_θ/K_0) with crack orientation for crack size $a = 0.4D$.

where first integral corresponds to $\bar{c}_{440}$, and similarly the second integral corresponds to $\bar{c}_{550}$. Incidentally, $\bar{c}_{440}$ and $\bar{c}_{550}$ represent compliances corresponding to 0° crack orientation angle. Hence,

$$\bar{c}_{44\theta} = \bar{c}_{440}\cos^2\theta + \bar{c}_{550}\sin^2\theta - \bar{c}_{450}\ \sin\ \theta\cos\ \theta \tag{28}$$

Similarly starting from Eq. (13) the following relation is obtained:

$$\bar{c}_{55\theta} = \bar{c}_{550}\cos^2\theta + \bar{c}_{440}\sin^2\theta + \bar{c}_{450}\ \sin\ \theta\cos\ \theta \tag{29}$$

This gives rise to an important relation for such a case

$$\bar{c}_{440} + \bar{c}_{550} = \bar{c}_{44\theta} + \bar{c}_{55\theta} \tag{30}$$

Again from Eq. (29), noting that $\bar{c}_{450} = 0$,

$$\bar{c}_{55\theta} = \bar{c}_{550}\left(\cos^2\theta + \frac{\bar{c}_{440}}{\bar{c}_{550}}\sin^2\theta\right) \tag{31}$$

Noting that $\bar{K}_{55\theta} = \bar{K}_{\theta} = 1/\bar{c}_{55\theta}$, $\bar{K}_{550} = \bar{K}_0 = 1/\bar{c}_{550}$ and $\bar{K}_{440} = \bar{K}_{90} = 1/\bar{c}_{440}$, this relation is the same as Eq. (26).

The rotational spring stiffness therefore increases with θ. The variation of dimensionless rotational spring stiffness with θ is shown in Fig. 7 for a long cantilever beam with the following dimensions and material data: Shaft diameter $D = 0.04$ m, length $L = 0.8$ m, crack located at $0.2L$ from the fixed end, crack depth $a = 0.4D$, $E = 200$ GPa, $\rho = 7800\,\mathrm{kg\,m^{-3}}$ and $v = 0.3$. The stiffnesses were computed for five orientations, 0°, 30°, 45°, 60°, 70°, 80° and 90°, by displacement method [28] through 3D FE analysis using ANSYS (version 9.0) software. Discretisation consisted of all 'Solid95' elements.

The FE results are included in Fig. 7. There is very good agreement between theoretical and FE results. The maximum difference observed is 8.4% at $\theta = 45°$.

4. Natural frequencies of Timoshenko (short) beam with crack

For a cantilever shaft beam with a crack in an arbitrary orientation with the vertical axis y and located at a distance L_c from the fixed end (Fig. 8), any arbitrary excitation of the shaft, except about the axis of symmetry of the crack-section, causes its free transverse vibrations in both y and z directions and torsion vibrations about x axis. Since the cross section at the crack-section is asymmetric with respect to y and z axes, there are triply coupled vibrations. That is, two transverse vibrations are coupled; the two transverse vibrations are coupled individually with the torsion vibration. When crack is oriented at $\theta = 0°$ or 90° the vibrations are doubly coupled because the two transverse vibrations are uncoupled.

To model the vibration of the shaft beam (Fig. 8) it can be split into two segments, AB and BC. The motion of each segment can be separately studied and their individual motions can be connected through compliance matrix noting that there are local incompabilities. The equations of two transverse vibrations and torsion vibration for each segment are given by equations of the type as follows:

$$EI\frac{\partial^4 Y(x,t)}{\partial x^4} + A_s\rho\frac{\partial^2 Y(x,t)}{\partial t^2} - \rho I\left(1 + \frac{E}{k'G}\right)\frac{\partial^4 Y(x,t)}{\partial x^2\,\mathrm{d}t^2} + \left(\frac{\rho^2 I}{k'G}\right)\frac{\partial^4 Y(x,t)}{\partial t^4} = 0 \tag{32}$$

$$EI\frac{\partial^4 Z(x,t)}{\partial x^4} + A_s\rho\frac{\partial^2 Z(x,t)}{\partial t^2} - \rho I\left(1 + \frac{E}{k'G}\right)\frac{\partial^4 Z(x,t)}{\partial x^2\,\partial t^2} + \left(\frac{\rho^2 I}{k'G}\right)\frac{\partial^4 Z(x,t)}{\partial t^4} = 0 \tag{33}$$

$$\frac{\partial^2 \Theta(x,t)}{\partial x^2} - \frac{\rho}{G}\frac{\partial^2 \Theta(x,t)}{\partial t^2} = 0 \tag{34}$$

where Y, Z and Θ stand for the displacement mode shapes in y, z and θ directions, respectively, A_s is area of cross section, ρ is material density, E is modulus of elasticity, $k' = 6(1+v)/(7+6v)$ is shape coefficient for circular cross section, G is modulus of rigidity and I is moment of inertia of the beam cross section.

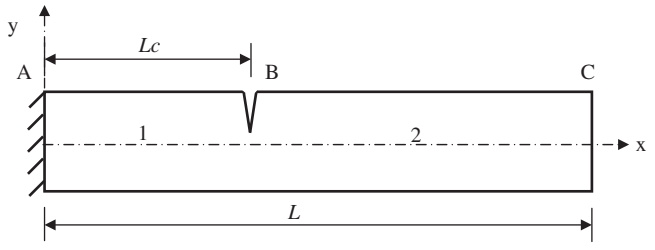

Fig. 8. Cantilever shaft beam with crack.

Through separation of variables the solutions are obtained following the procedure of Ref. [18] as follows:

$$\left.\begin{aligned} Y_1 &= C_1\cosh(bp\beta) + C_2\sinh(bp\beta) + C_3\cos(bq\beta) + C_4\sin(bq\beta)\\ \psi_1 &= C_1'\sinh(bp\beta) + C_2'\cosh(bp\beta) + C_3'\sin(bq\beta) + C_4'\cos(bq\beta)\\ Y_2 &= C_5\cosh(bp\beta) + C_6\sinh(bp\beta) + C_7\cos(bq\beta) + C_8\sin(bq\beta)\\ \psi_2 &= C_5'\sinh(bp\beta) + C_6'\cosh(bp\beta) + C_7'\sin(bq\beta) + C_8'\cos(bq\beta) \end{aligned}\right\} \tag{35}$$

$$\left.\begin{aligned} Z_1 &= C_9\cosh(bp\beta) + C_{10}\sinh(bp\beta) + C_{11}\cos(bq\beta) + C_{12}\sin(bq\beta)\\ \phi_1 &= C_9'\sinh(bp\beta) + C_{10}'\cosh(bp\beta) + C_{11}'\sin(bq\beta) + C_{12}'\cos(bq\beta)\\ Z_2 &= C_{13}\cosh(bp\beta) + C_{14}\sinh(bp\beta) + C_{15}\cos(bq\beta) + C_{16}\sin(bq\beta)\\ \phi_2 &= C_{13}'\sinh(bp\beta) + C_{14}'\cosh(bp\beta) + C_{15}'\sin(bq\beta) + C_{16}'\cos(bq\beta) \end{aligned}\right\} \tag{36}$$

$$\left.\begin{aligned} \bar{\Theta}_1 &= C_{17}\cos(\bar{k}_\theta\beta) + C_{18}\sin(\bar{k}_\theta\beta)\\ \bar{\Theta}_2 &= C_{19}\cos(\bar{k}_\theta\beta) + C_{20}\sin(\bar{k}_\theta\beta) \end{aligned}\right\} \tag{37}$$

where C_i ($i = 1$ to 20) and C_i' ($i = 1$ to 16) are all arbitrary constants, $\beta = L_c/L$ and, ψ and ϕ are the slopes of the deflection curves in the x–y (vertical) and x–z (horizontal) planes, respectively, suffixes 1 and 2 stand for segments AB and BC, respectively, and

$$C_i' = \frac{b}{L}\frac{p^2+s^2}{p}C_i \quad \text{for } i = 1,2,5,6,9,10,13 \text{ and } 14 \tag{38}$$

$$C_i' = -\frac{b}{L}\frac{q^2-s^2}{q}C_i \quad \text{for } i = 3,7,11 \text{ and } 15 \tag{39}$$

$$C_i' = \frac{b}{L}\frac{q^2-s^2}{q}C_i \quad \text{for } i = 4,8,12 \text{ and } 16 \tag{40}$$

$$b^2 = \frac{\rho AL^4\omega^2}{EI}, \quad s^2 = \frac{EI}{k'AGL^2}$$

$$\left.\begin{matrix} q\\ p \end{matrix}\right\} = \frac{1}{\sqrt{2}}\left\{\pm(r^2+s^2) + \left[(r^2-s^2)^2 + \frac{4}{b^2}\right]^{1/2}\right\}^{1/2} \tag{41}$$

and

$$r^2 = \frac{I}{AL^2} \text{ provided } \left[(r^2-s^2)^2 + \frac{4}{b^2}\right]^{1/2} > (r^2+s^2)$$

$$\bar{\Theta} = \frac{\Theta}{L} \tag{42}$$

$$\bar{k}_\theta = \frac{\omega^2L^2\rho}{G} \tag{43}$$

The boundary conditions for a cantilever configuration, in dimensionless form, are given below.

At the fixed end ($\beta = 0$) all displacements, slopes and angle of twist are zero.

$$Y_1 = 0, \quad Z_1 = 0, \quad \psi_1 = 0, \quad \phi_1 = 0, \quad \bar{\Theta}_1 = 0 \tag{44a–e}$$

At the free end ($\beta = 1$), moments in the two planes, shear forces in the two directions and torque are zero. That is,

$$\frac{d\psi_2}{d\beta} = 0, \quad \frac{d\phi}{d\beta} = 0, \quad \frac{1}{L}\frac{dY_2}{d\beta} - \psi_2 = 0, \quad \frac{1}{L}\frac{dZ_2}{d\beta} - \phi_2 = 0, \quad \frac{d\bar{\Theta}}{d\beta} = 0 \quad \text{at } \beta = 1 \tag{45a–e}$$

At the crack location $\beta = \beta_1$ the continuity conditions in terms of two moments, two shear forces and torque are as follows:

$$\left.\frac{d\psi_1}{d\beta}=\frac{d\psi_2}{d\beta},\quad \frac{d\phi_1}{d\beta}=\frac{d\phi_2}{d\beta},\quad \frac{1}{L}\frac{dY_1}{d\beta}-\psi_1=\frac{1}{L}\frac{dY_2}{d\beta}-\psi_2,\quad \frac{1}{L}\frac{dZ_1}{d\beta}-\phi_1=\frac{1}{L}\frac{dZ_2}{d\beta}-\phi_2,\quad \frac{d\bar{\Theta}_1}{d\beta}=\frac{d\bar{\Theta}_2}{d\beta}\right\} \tag{46a–e}$$

At this location, the jump conditions in slope and shear rotation in the two cartesian directions, and angle of twist can be represented by

$$\left.\begin{aligned}
&\frac{EI}{L}\frac{d\psi_1}{d\beta}=k_{55}(\psi_2-\psi_1)+k_{54}(\phi_2-\phi_1)\\
&\frac{EI}{L}\frac{d\phi_1}{d\beta}=k_{44}(\phi_2-\phi_1)+k_{45}(\psi_2-\psi_1)\\
&k'GA\left(\frac{1}{L}\frac{dY_1}{d\beta}-\psi_1\right)=k_{33}(Y_2-Y_1)+Lk_{36}(\bar{\Theta}_2-\bar{\Theta}_1)+k_{32}(Z_2-Z_1)\\
&k'GA\left(\frac{1}{L}\frac{dZ_1}{d\beta}-\phi_1\right)=k_{22}(Z_2-Z_1)+Lk_{26}(\bar{\Theta}_2-\bar{\Theta}_1)+k_{23}(Y_2-Y_1)\\
&GI_p\frac{d\bar{\Theta}_1}{d\beta}=Lk_{66}(\bar{\Theta}_2-\bar{\Theta}_1)+k_{62}(Z_2-Z_1)+k_{63}(Y_2-Y_1)
\end{aligned}\right\} \tag{47a–e}$$

where k_{ij}'s are the stiffness matrix coefficients.

Eqs. (47a and b) are related to jump in slope of the deflection curves; Eqs. (47c and d) are related to jump in shear deformations; and Eq. (47e) is concerned with discontinuity in the angle of twist.

Substituting Eqs. (35)–(37) in the above conditions give the characteristic determinant of size 20×20. Roots of the characteristic equation give the transverse natural frequencies in the vertical and horizontal planes and torsion frequencies.

5. Natural frequencies of Euler–Bernoulli (long) beam with crack

In case of Euler–Bernoulli cantilever beam, the shear deformations can be neglected. Therefore, for such a beam with a crack located at a distance L_c from the fixed support, the equations of two transverse vibrations (in the y and z directions) and torsion vibration for each segment are given by equation of the following type:

$$\frac{\partial^4 Y(x,t)}{\partial x^4}+\frac{A_s\rho}{EI}\frac{\partial^4 Y(x,t)}{\partial t^4}=0 \tag{48}$$

$$\frac{\partial^4 Z(x,t)}{\partial x^4}+\frac{A_s\rho}{EI}\frac{\partial^4 Z(x,t)}{\partial t^4}=0 \tag{49}$$

$$\frac{\partial^2 \Theta(x,t)}{\partial x^2}-\frac{\rho}{G}\frac{\partial^2 \Theta(x,t)}{\partial t^2}=0 \tag{50}$$

As before, the solutions for Eqs. (48)–(50) are obtained through the method of separation of variables. The mode shapes for the two segments are as follows.

$$\left.\begin{aligned}
Y_1&=C_1\cosh(\lambda\beta)+C_2\sinh(\lambda\beta)+C_3\cos(\lambda\beta)+C_4\sin(\lambda\beta)\\
Y_2&=C_5\cosh(\lambda\beta)+C_6\sinh(\lambda\beta)+C_7\cos(\lambda\beta)+C_8\sin(\lambda\beta)\\
Z_1&=C_9\cosh(\lambda\beta)+C_{10}\sinh(\lambda\beta)+C_{11}\cos(\lambda\beta)+C_{12}\sin(\lambda\beta)\\
Z_2&=C_{13}\cosh(\lambda\beta)+C_{14}\sinh(\lambda\beta)+C_{15}\cos(\lambda\beta)+C_{16}\sin(\lambda\beta)
\end{aligned}\right\} \tag{51}$$

$$\left.\begin{aligned}
\bar{\Theta}_1&=C_{17}\cos(\bar{k}_\theta\beta)+C_{18}\sin(\bar{k}_\theta\beta)\\
\bar{\Theta}_2&=C_{19}\cos(\bar{k}_\theta\beta)+C_{20}\sin(\bar{k}_\theta\beta)
\end{aligned}\right\} \tag{52}$$

where C_i ($i = 1$ to 20) are all arbitrary constants and $\lambda^4 = \rho AL^4\omega^2/EI$. The boundary conditions in terms of deflections, slopes and angle of twist at the fixed end ($\beta = 0$) are given by

$$Y_1 = 0, \quad Z_1 = 0, \quad \frac{dY_1}{d\beta} = 0, \quad \frac{dZ_1}{d\beta} = 0, \quad \bar{\Theta}_1 = 0 \tag{53a–e}$$

At the free end ($\beta = 1$), bending moments, shear forces and twisting moment are zero. Therefore,

$$\frac{d^2Y_2}{d\beta^2} = 0, \quad \frac{d^2Z_2}{d\beta^2} = 0, \quad \frac{d^3Y_2}{d\beta^3} = 0, \quad \frac{d^3Z_2}{d\beta^3} = 0, \quad \frac{d\bar{\Theta}_2}{d\beta} = 0 \quad \text{at } \beta = 1 \tag{54a–e}$$

The continuity of displacements, bending moments, shear forces and twisting moment at the crack location $\beta = \beta_1$ are as follows:

$$Y_1 = Y_2, \quad Z_1 = Z_2, \quad \frac{d^2Y_1}{d\beta^2} = \frac{d^2Y_2}{d\beta^2}, \quad \frac{d^2Z_1}{d\beta^2} = \frac{d^2Z_2}{d\beta^2}, \quad \frac{d^3Y_1}{d\beta^3} = \frac{d^3Y_2}{d\beta^3}, \quad \frac{d^3Z_1}{d\beta^3} = \frac{d^3Z_2}{d\beta^3}, \quad \frac{d\bar{\Theta}_1}{d\beta} = \frac{d\bar{\Theta}_2}{d\beta} \tag{55a–g}$$

The jump conditions at the crack location $\beta = \beta_1$ can be written in the following form:

$$\left.\begin{aligned} EI\frac{d^2Y_1}{d\beta^2} &= k_{55}\left(\frac{dY_2}{d\beta} - \frac{dY_1}{d\beta}\right) + k_{54}\left(\frac{dZ_2}{d\beta} - \frac{dZ_1}{d\beta}\right) \\ EI\frac{d^2Z_1}{d\beta^2} &= k_{44}\left(\frac{dZ_2}{d\beta} - \frac{dZ_1}{d\beta}\right) + k_{45}\left(\frac{dY_2}{d\beta} - \frac{dY_1}{d\beta}\right) \\ GI_p\frac{d\bar{\Theta}}{d\beta} &= Lk_{66}(\bar{\Theta}_2 - \bar{\Theta}_1) \end{aligned}\right\} \tag{56a–c}$$

where k_{ij}'s are the stiffness matrix coefficients.

As opposed to the Timoshenko beam, though the Euler–Bernoulli beam vibrates in the three directions y, z and θ, only the two transverse vibrations are coupled and there is no torsion–transverse vibration coupling. Again substituting Eqs. (51) and (52) in the boundary, compatibility and jump condition give the 20×20 characteristic determinant. Roots of the determinant obtained by equating it to zero give the natural transverse and torsion vibration frequencies.

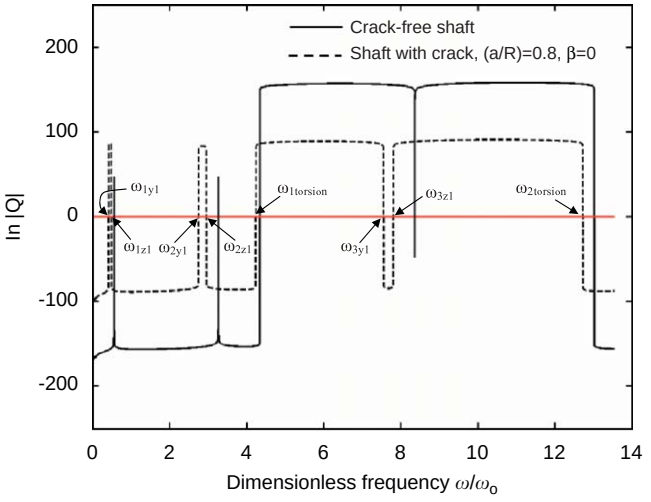

Fig. 9. Variation of characteristic determinant with ω/ω_0 for Timoshenko beam for $\theta = 15°$.

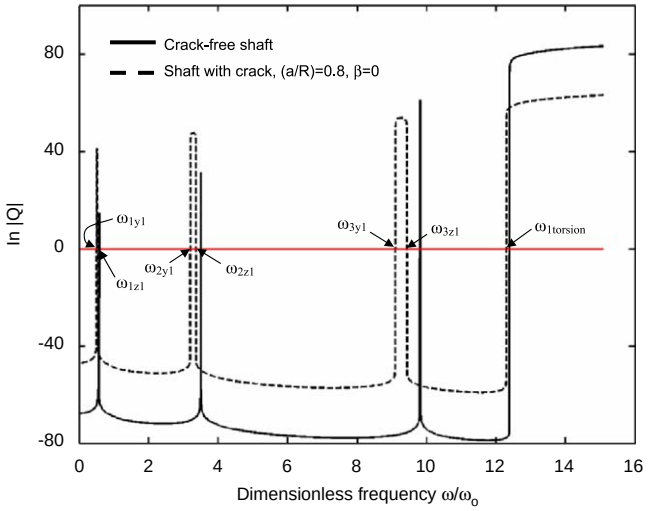

Fig. 10. Variation of characteristic determinant with ω/ω_0 for Euler–Bernoulli beam for $\theta = 15^\circ$.

6. Case studies

The following sets of data are employed for the case studies: $L = 0.8\,\text{m}$ for Euler–Bernoulli beam, $L = 0.28\,\text{m}$ for Timoshenko beam, shaft diameter D (or $2R$) $= 0.04\,\text{m}$, $E = 200\,\text{GPa}$, $\rho = 7800\,\text{kg m}^{-3}$ and $v = 0.3$. Variations of $\ln|Q|$, where $|Q|$ is the 20×20 characteristic determinant, with the dimensionless frequency (ω/ω_0) for the Timoshenko and Euler–Bernoulli beams are shown in Figs. 9 and 10, respectively, for $\theta = 15^\circ$. The normalising frequency $\omega_0 = \sqrt{EI/(\rho AL^4)}$. It is to be noted that ω_0 for the Euler–Bernoulli and Timoshenko beams are different.

The natural frequencies for a crack-free beam are computed by setting all the compliance coefficients to 0 in the compliance matrix. Alternatively, the same frequencies can be obtained by setting all the stiffness coefficients as ∞.

Three transverse and two torsion frequencies for the Timoshenko beam considered here fall within the range shown in Fig. 9; three transverse and one torsion frequencies for the Euler–Bernoulli beam studied fall within the range shown in Fig. 10. The transverse frequencies corresponding to the y and z directions are closely-spaced for a particular mode.

The transverse frequencies in the vertical (ω_{iy}) and horizontal (ω_{iz}) directions do not change with crack orientation θ (Table 1) in the case of both short and long beams for $a/R = 0.6$ for three modes. These frequencies were also computed using ANSYS software and are included in the same table. FE results too indicate that the frequencies do not change with angle θ.

The variations of transverse natural frequencies with crack locations and depths for the Timoshenko ($L/D = 20$) and Euler–Bernoulli ($L/D = 7$) beams are shown in Fig. 11. Similar plots for torsion frequncies are presented in Fig. 12. As expected, all the frequencies decrease as the crack depth increases; the change in a frequency reduces as the crack location shifts towards the free end. These plots show trends similar to the ones reported in Refs. [31,32]. Reductions in all the transverse and torsion natural frequecies for a Timoshenko beam have been found to be more in comparision with those for an Euler–Bernoulli beam.

The vibration of the shaft beam in the vertical plane, when modelled using a single rotational spring, indicates that the frequencies are dependent with angle θ (Table 2). This is completely contradictory to what is obseved through the triply coupled analysis.

7. Discussion and conclusions

Analyses for the free transverse and torsion vibrations of Timoshenko (short) and Euler–Bernoulli (long) shaft beams with an open planar edge crack in an arbitrary orientation have been presented. Coupled

Table 1
Natural frequecies obtained analytically and using EEM for short and long beams.

Crack-free shaft ω_i	Mode identity	FEM	Analytical				
		ω_i for $\theta = 0^\circ$	ω_i for $\theta = 0^\circ$	ω_i for $\theta = 15^\circ$	ω_i for $\theta = 45^\circ$	ω_i for $\theta = 75^\circ$	ω_i for $\theta = 90^\circ$
Short beam ($a/R = 0.6$ and $\beta = 0.1$)							
357.3028	ω_{1y}	319.06	315.37	315.37	315.37	315.37	315.37
	ω_{1z}	352.60	344.49	344.49	344.49	344.49	344.49
2101.641	ω_{2y}	2044.89	2033.92	2033.92	2033.92	2033.92	2033.92
	ω_{2z}	2095.66	2079.12	2079.12	2079.12	2079.12	2079.12
2803.9116	$\omega_{1\,\text{torsion}}$	2743.09	2766.67	2766.67	2766.67	2766.67	2766.67
5409.1991	ω_{3y}	5411.64	5389.54	5389.54	5389.54	5389.54	5389.54
	ω_{3z}	5424.15	5401.16	5401.16	5401.16	5401.16	5401.16
8411.5772	$\omega_{2\,\text{torsion}}$	8263.25	8321.97	8321.97	8321.97	8321.97	8321.97
Long beam ($a/R = 0.4$ and $\beta = 0.1$)							
44.2451	ω_{1y}	42.29	42.57	42.57	42.57	42.57	42.57
	ω_{1z}	44.02	43.85	43.85	43.85	43.85	43.85
277.4071	ω_{2y}	270.85	273.67	273.67	273.67	273.67	273.67
	ω_{2z}	274.76	276.37	276.37	276.37	276.37	276.37
776.8353	ω_{3y}	758.36	775.00	775.00	775.00	775.00	775.00
	ω_{3z}	760.96	776.28	776.28	776.28	776.28	776.28
981.2712	$\omega_{1\,\text{torsion}}$	973.94	976.81	976.81	976.81	976.81	976.81

equations of motion have been derived. The compliance matrix coefficients in terms of the angular position of crack have been determined. Typical variation of the compliance coefficients with angular orientation of crack has been presented. Existence of a coupling between shear deformations along the two in-plane axes has been illustrated. The transverse frequencies in the vertical and horizontal directions and torsion frequencies have been obtained for a few cases and have been verified by comparing with results based on finite element (FE) analysis. These show that the frequencies are independent of crack orientation, when the full compliance matrix is employed. The transverse frequency in one plane determined through representation of the crack by a single rotational spring may, however, show dependencies on crack orientation. Variation of the stiffness of such a single spring with the crack orientation for a particular crack size is included and it has been compared with FE results; there is a very good agreement. Natural frequencies of both Timoshenko and Euler–Bernoulli beams in the vertical and horizontal directions and torsion frequencies have been found to reduce, as expected, with crack depth. The extent of reduction is inversely related to the crack distance from the fixed end. These changes may be exploited to solve the inverse problem. Thus, the data presented here will be useful for analyzing the forward and inverse problems. It is important to note here that the localised crack model through the compliance approach is a convenient way of representing a crack. However, it should not be indiscriminately employed in situations, where the underlying assumptions of the model are violated. The main assumptions are that the influence of crack is localised and its effect can be expressed fully through the SIFs.

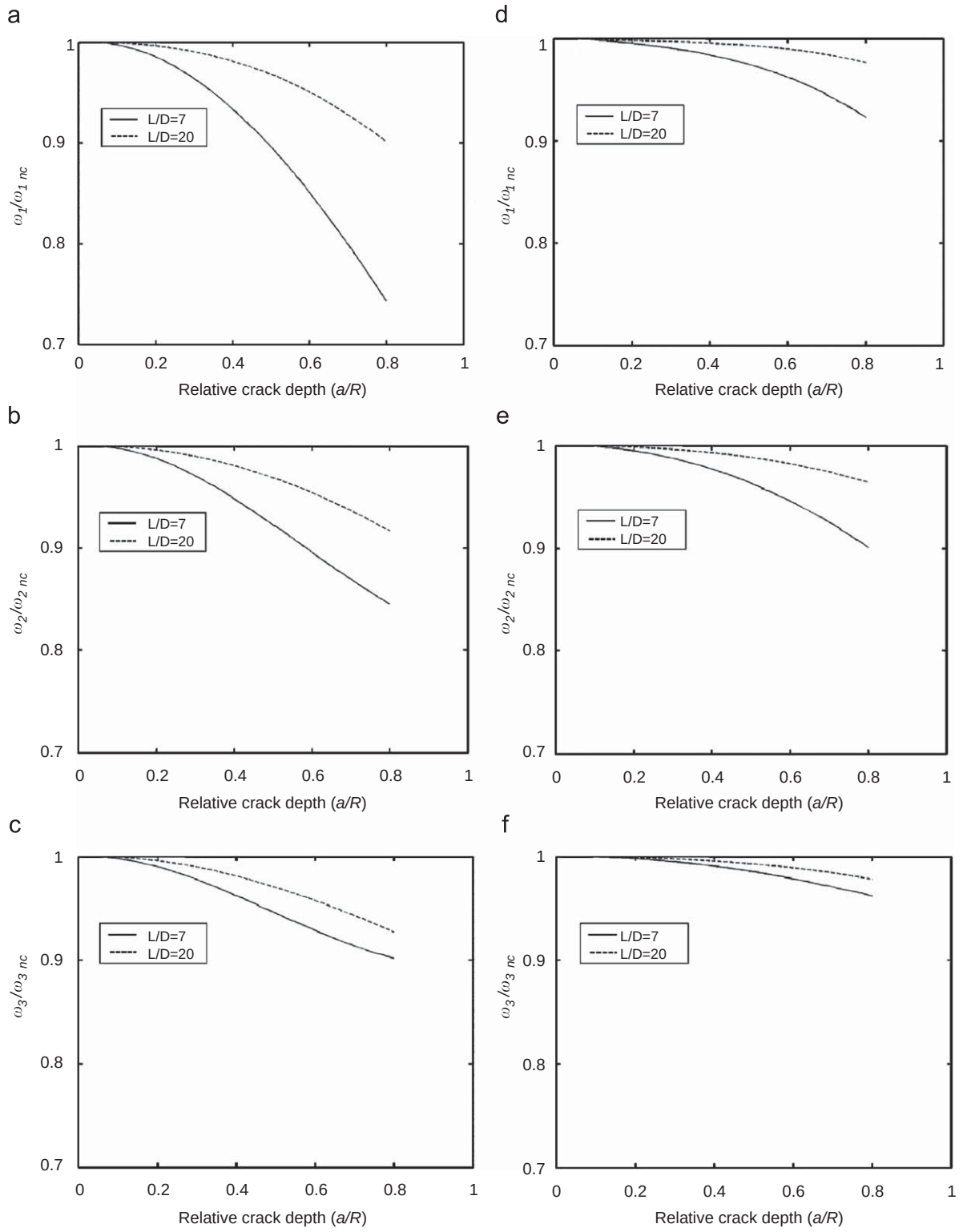

Fig. 11. Variation of first three transverse frequencies with relative crack depth for Timoshenko ($L/D = 7$) and Euler–Bernoulli ($L/D = 20$) beams. (a), (b) and (c) crack located at fixed end ($\beta = 0$). (d), (e) and (f) Crack located at $0.4L$ from fixed end.

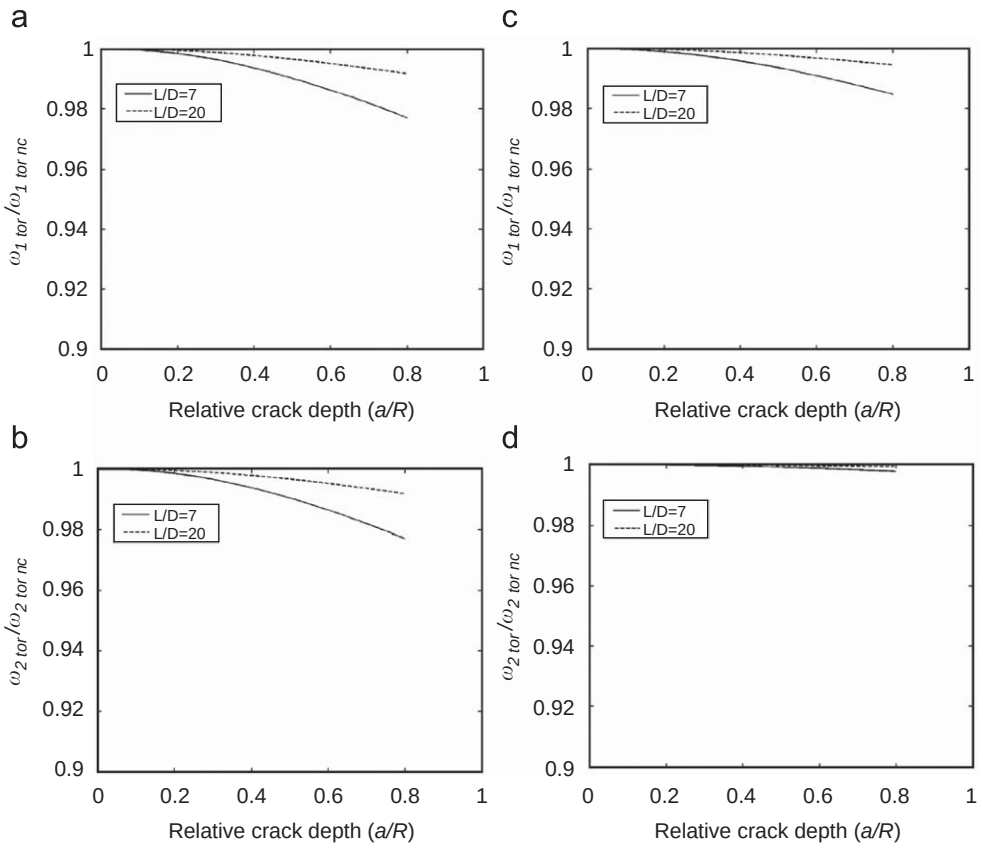

Fig. 12. Variation of first two torsion frequencies with relative crack depth for Timoshenko ($L/D = 7$) and Euler–Bernoulli ($L/D = 20$) beams. (a) and (b) Crack located at fixed end ($\beta = 0$). (c) and (d) Crack located at $0.4L$ from fixed end.

Table 2
First three transverse natural frequencies for short and long beams in vertical (y-x) plane obtained with single rotational spring model.

Crack-free shaft ω_i	ω_i for $\theta = 0^\circ$	ω_i for $\theta = 15^\circ$	ω_i for $\theta = 45^\circ$	ω_i for $\theta = 75^\circ$	ω_i for $\theta = 90^\circ$
Short beam ($a/R = 0.6$ and $\beta = 0.1$)					
357.3028	315.37	320.94	337.65	343.86	344.49
2101.641	2033.92	2042.04	2067.98	2078.17	2079.28
5409.1991	5389.54	5391.93	5399.73	5402.91	5403.23
Long beam ($a/R = 0.4$ and $\beta = 0.1$)					
44.2451	42.58	42.89	43.53	43.84	43.84
277.4071	273.67	274.30	275.74	276.37	276.37
776.8353	775.00	775.17	775.97	776.28	776.28

References

[1] J. Wauer, Cracked rotor dynamics: a state of the art survey, *Applied Mechanics Reviews* 43 (1) (1990) 13–17.
[2] R. Gasch, A survey of the dynamic behaviour of a simple rotating shaft with a transverse crack, *Journal of Sound and Vibration* 160 (2) (1993) 313–332.
[3] A.D. Dimarogonas, Vibration of cracked structures: a state of the art review, *Engineering Fracture Mechanics* 55 (5) (1996) 831–857.
[4] C.A. Papadopoulos, The strain energy release approach for modeling cracks in rotors: a state of the art review, *Mechanical Systems and Signal Processing* 22 (4) (2008) 763–789.

[5] A.D. Dimarogonas, G. Massouros, Torsional vibration of a shaft with a circumferential crack, *Engineering Fracture Mechanics* 15 (3–4) (1981) 439–444.
[6] C.A. Papadopoulos, A.D. Dimarogonas, Coupled longitudinal and bending vibrations of a rotating shaft with an open crack, *Journal of Sound and Vibration* 117 (1) (1987) 81–93.
[7] A.K. Darpe, K. Gupta, A. Chawla, Analysis of the response of a cracked Jeffcott rotor to axial excitation, *Journal of Sound and Vibration* 249 (3) (2002) 429–445.
[8] A.K. Darpe, K. Gupta, A. Chawla, Experimental investigations of the response of a cracked rotor to periodic axial excitation, *Journal of Sound and Vibration* 260 (2) (2003) 265–286.
[9] A.K. Darpe, K. Gupta, A. Chawla, Coupled bending, longitudinal and torsional vibrations of a cracked rotor, *Journal of Sound and Vibration* 269 (1–2) (2004) 33–60.
[10] S. Christides, A.D.S. Barr, One-dimensional theory of cracked Bernoulli–Euler beam, *International Journal of Mechanical Sciences* 26 (11/12) (1984) 639–648.
[11] S. Christides, A.D.S. Barr, Torsional vibration of cracked beams of non-circular cross-section, *International Journal of Mechanical Sciences* 28 (7) (1986) 473–490.
[12] M.-H.H. Shen, C. Pierre, Natural modes of Bernoulli–Euler beams with symmetric cracks, *Journal of Sound and Vibration* 138 (1) (1990) 115–134.
[13] T.G. Chondros, The continuous crack flexibility method for crack identification, *Fatigue and Fracture of Engineering Materials and Structures* 24 (4) (2001) 643–650.
[14] T.G. Chondros, Variational formulation of a rod under torsional vibration for crack identification, *Theoretical and Applied Fracture Mechanics* 44 (1) (2005) 95–104.
[15] T.G. Chondros, G.N. Labeas, Torsional vibration of a cracked rod by variational formulation and numerical analysis, *Journal of Sound and Vibration* 301 (3–5) (2007) 994–1006.
[16] B.P. Nandwana, S.K. Maiti, Modeling of vibration of beam in presence of inclined edge or internal crack for its possible detection based on frequency measurements, *Engineering Fracture Mechanics* 58 (3) (1997) 193–205.
[17] A.P. Bovsunovsky, V.V. Matveev, Analytical approach to the determination of dynamic characteristics of a beam with a closing crack, *Journal of Sound and Vibration* 235 (3) (2000) 415–434.
[18] S.P. Lele, S.K. Maiti, Modeling of transverse vibrations for crack detection and measurement of crack extension, *Journal of Sound and Vibration* 257 (3) (2002) 559–583.
[19] N. Dharmaraju, R. Tiwari, S. Talukdar, Identification of an open crack model in a beam based on force-response measurements, *Computers and Structures* 82 (2–3) (2004) 167–179.
[20] M.H.F. Dado, O. Abuzeid, Coupled transverse and axial vibratory behaviour of cracked beam with end mass and rotary inertia, *Journal of Sound and Vibration* 261 (4) (2003) 675–696.
[21] W.M. Ostachowicz, M. Krawczuk, Coupled torsional and bending vibration of a rotor with an open crack, *Archives of Applied Mechanics* 62 (3) (1992) 191–201.
[22] A.C. Chasalevris, C.A. Papadopoulos, Identification of multiples cracks in beams under bending, *Mechanical Systems and Signal Processing* 20 (7) (2006) 1631–1673.
[23] D.Y. Zheng, S.C. Fan, Vibration and stability of cracked hollow-sectional beams, *Journal of Sound and Vibration* 267 (4) (2003) 933–954.
[24] G. Gounaris, N. Anifantis, A.D. Dimarogonas, Dynamics of cracked hollow beams, *Engineering Fracture Mechanics* 39 (6) (1991) 931–940.
[25] G.D. Gounaris, C.A. Papadopoulos, Crack identification in rotating shafts by coupled response measurements, *Engineering Fracture Mechanics* 69 (3) (2002) 339–352.
[26] T.G. Chondros, A.D. Dimarogonas, J. Yao, Vibration of a beam with a breathing crack, *Journal of Sound and Vibration* 239 (1) (2001) 57–67.
[27] D.Y. Zheng, N.J. Kessissoglou, Free vibration analysis of a cracked beam by finite element method, *Journal of Sound and Vibration* 273 (3) (2004) 457–475.
[28] M.R. Naniwadekar, S.S. Naik, S.K. Maiti, On prediction of crack in different orientations in pipe using frequency based approach, *Mechanical Systems and Signal Processing* 22 (3) (2008) 693–708.
[29] K.M. Saridakis, A.C. Chasalevris, C.A. Papadopoulos, A.J. Dentsoras, Applying neural network genetic algorithm and fuzzy logic for identification of cracks in shafts by using coupled response measurements, *Computers and Structures* 86 (11–12) (2008) 1318–1338.
[30] A.D. Dimoarogonas, C.A. Papadopoulos, Vibration of cracked shaft in bending, *Journal of Sound and Vibration* 91 (4) (1983) 583–593.
[31] M.D. Rajab, A. Al-Sabeeh, Vibration characteristics of cracked shafts, *Journal of Sound and Vibration* 147 (3) (1991) 465–473.
[32] A.S. Sekhar, B.S. Prabhu, Crack detection and vibration characteristics of cracked shafts, *Journal of Sound and Vibration* 157 (2) (1992) 375–381.